RSC Advances

PAPER

View Article Online
View Journal | View Issue

Cite this: *RSC Adv.*, 2026, **16**, 19312

Theoretical study on the geometry, aromaticity and electronic properties of porphyrin analogues

Xiahe Chen,[a] Dawei Li,[a] Chengwei Zhang,[a] Yuanbin She *[ab] and Yun-Fang Yang *[ac]

Received 19th January 2026
Accepted 6th April 2026

DOI: 10.1039/d6ra00486e

rsc.li/rsc-advances

Density functional theory calculations were employed to investigate a family of porphyrin analogues differing in macrocyclic size and bridging motif. The geometrical features of these macrocycles exhibit pronounced variations in bond lengths, bond angles, and overall conformations as the framework size and linkage patterns are altered. Nucleus independent chemical shift (NICS) values and anisotropy of the induced current density (AICD) analyses were calculated to evaluate the aromaticity of the porphyrin analogues. The porphyrin analogues exhibit pronounced aromatic character. The electronic properties were further examined by frontier molecular orbital analysis, revealing systematic changes in orbital energies with increasing π-conjugation length and with nitrogen substitution at the *meso* positions. We expect that these studies will provide new insights and will aid the further development of diverse novel porphyrin analogues.

Introduction

Macrocyclic complexes have attracted considerable attention in bioinorganic chemistry, with porphyrins representing one of the most extensively studied classes. Porphyrins consist of four pyrrolic subunits, in which the pyrrole rings are interconnected through methine carbons at the *meso* positions.[1] In nature, porphyrin frameworks participate in numerous essential biological processes, including photosynthesis in chlorophyll, oxygen transport in hemoglobin, and oxygen storage in myoglobin, earning them the designation "pigments of life".[2] Beyond their biological significance, synthetic porphyrins have also been widely investigated because of their broad applications in diverse fields.[3] In addition, recent studies have employed machine-learning approaches to predict properties based on existing porphyrin databases.[4]

Porphyrin macrocycles exhibit a wide variety of structural variants, which can be generated by altering the number of pyrrole rings, substituting pyrrolic nitrogen atoms with other heteroatoms, replacing *meso*-carbon atoms with heteroatoms, or adding or removing *meso*-carbons from the macrocycle, among other modifications.[5] Representative examples include contracted porphyrins,[6] expanded porphyrins,[7] and heteroporphyrins[8] (Scheme 1). Such structural modifications profoundly influence the intrinsic properties of the macrocycle, including its cavity size, degree of planarity, π-electron configuration, and aromatic character.[9] For example, expanded porphyrins possess enlarged ring frameworks that extend the π-conjugated system, resulting in bathochromic shifts in their absorption spectra. The nonlinear optical (NLO) properties of these compounds have been extensively investigated, revealing that their NLO responses and excited-state dynamics are closely related to structural variations and to their aromatic or antiaromatic character, which is influenced by the total number of π-electrons.[10] In heteroporphyrin systems, our previous theoretical studies have shown that regular porphyrins and *O*-substituted porphyrins follow a 22π-electron aromaticity model, whereas heteroporphyrins substituted with PH, AsH, S, Se, Te, CH_2, or SiH_2 conform to an 18π-[18]annulene aromaticity model.[11] The aromaticity of porphyrin analogues has been investigated,[12,13] and recent reviews have summarized the methodologies used to assess the aromatic character of expanded porphyrins.[14]

Although porphyrins themselves have been extensively investigated, the structure–property relationships of their analogues remain insufficiently understood and have not yet been systematically characterized. This makes it difficult to elucidate functional regulatory mechanisms at the molecular level and to further expand their practical applications across diverse fields. To address these issues, the present study provides a detailed theoretical investigation of porphyrin analogues, with the aim of establishing a rational basis for their future molecular design and functional development. The porphyrin analogues considered in this work are illustrated in Scheme 1 and classified according to the number of pyrrole rings and methine carbon atoms. In groups **A–D**, the number of

[a]*College of Chemical Engineering, Zhejiang University of Technology, Hangzhou, Zhejiang 310014, China. E-mail: sheyb@zjut.edu.cn; yangyf@zjut.edu.cn*

[b]*State Key Laboratory of Green Chemical Synthesis and Conversion, Hangzhou 310014, China*

[c]*Zhejiang Key Laboratory of Surface and Interface Science and Engineering for Catalysts, Hangzhou 310014, China*

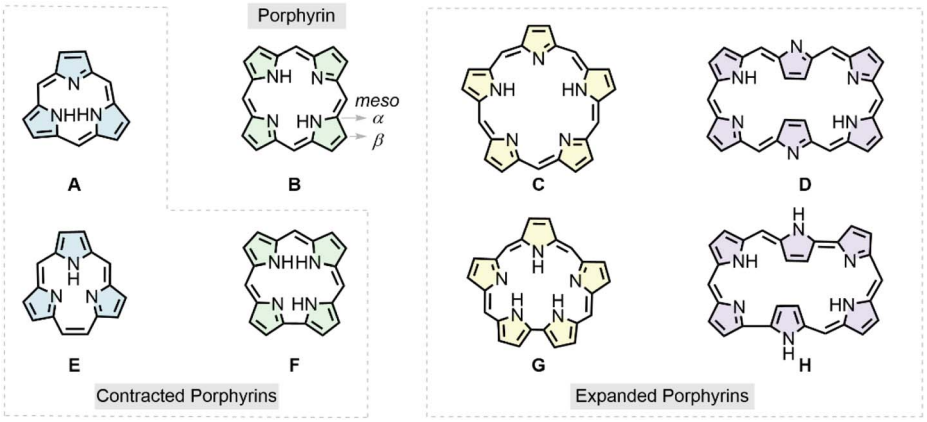

Scheme 1 Structures of porphyrin analogues investigated in this study.

pyrrole rings increases stepwise from three to six, with adjacent units connected through *meso*-atom bridges. Groups **E–H** also contain three to six pyrrole rings but involve the insertion or removal of one or two atoms at the *meso* positions. In addition, porphyrazine analogues are included in each group, in which the *meso*-carbons atoms are replaced by nitrogen atoms.

Computational methods

All calculations were performed using the Gaussian 16 package.[15] Geometry optimizations and energy calculations were carried out with B3LYP-D3,[16] which has been widely applied in computational studies of porphyrin systems.[17] The def2-SVP basis set[18] was used for all atoms. Frequency analysis was conducted at the same level of theory to verify that the stationary points are minima or saddle points. Computed structures were visualized using CYLview.[19] The molecular planarity parameter (MPP)[20] was calculated using Multiwfn.[21]

Frontier molecular orbitals (FMOs) and their energies were calculated at the HF/def2-TZVP[22] level using the gas-phase optimized geometries. Both nucleus independent chemical shifts (NICS)[23] values and anisotropy of the induced current density (AICD)[24] analyses were computed at the B3LYP-D3/def2-TZVP level on the same geometries. For NICS calculations of both planar and nonplanar structures, the reference plane was defined by least-squares fitting to the heavy atoms of the macrocycle, and the ring center was determined accordingly. NICS(0) values were obtained at the geometrical center of the heavy atoms, while NICS(1) values correspond to the average of values calculated 1 Å above and below the ring center. Aromatic species exhibit negative NICS values and clockwise induced current densities, whereas antiaromatic species show positive NICS values and counterclockwise currents.

Results and discussion

Geometry of porphyrin analogues

The optimized structures of the corresponding porphyrin analogues **A1–D1** are shown in Fig. 1. Across this series, the average bond lengths of the α-$C_{pyrrole}$–C_{meso} (*meso*-methine

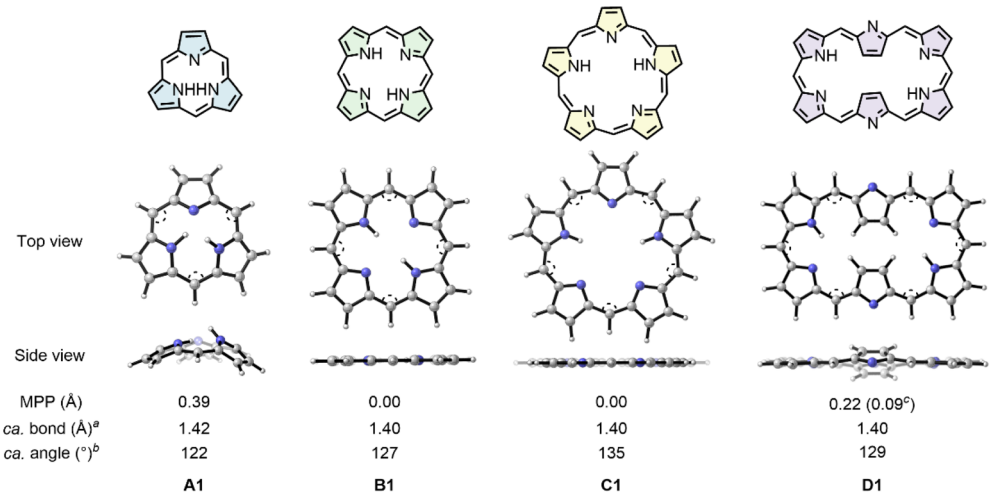

Fig. 1 Optimized geometries of porphyrin analogues **A1–D1**. [a]average bond length of all *meso*-methine bridges; [b]average bond angle of all *meso*-methine bridges; [c]C_β atoms of flipped pyrrole rings excluded from MPP calculations.

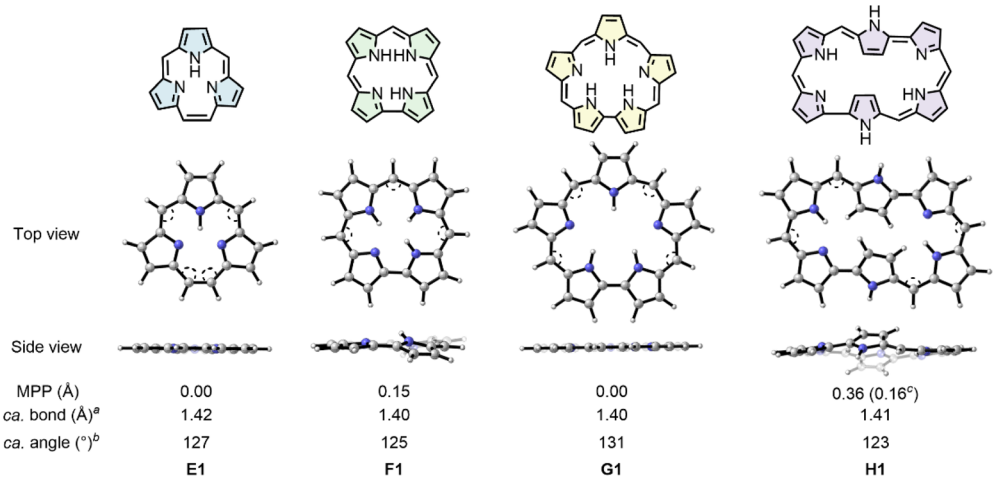

Fig. 2 Optimized geometries of porphyrin analogues **E1–H1**. [a]Average bond length of all *meso*-methine bridges; [b]average bond angle of all *meso*-methine bridges; [c]C_β atoms of flipped pyrrole rings excluded from MPP calculations.

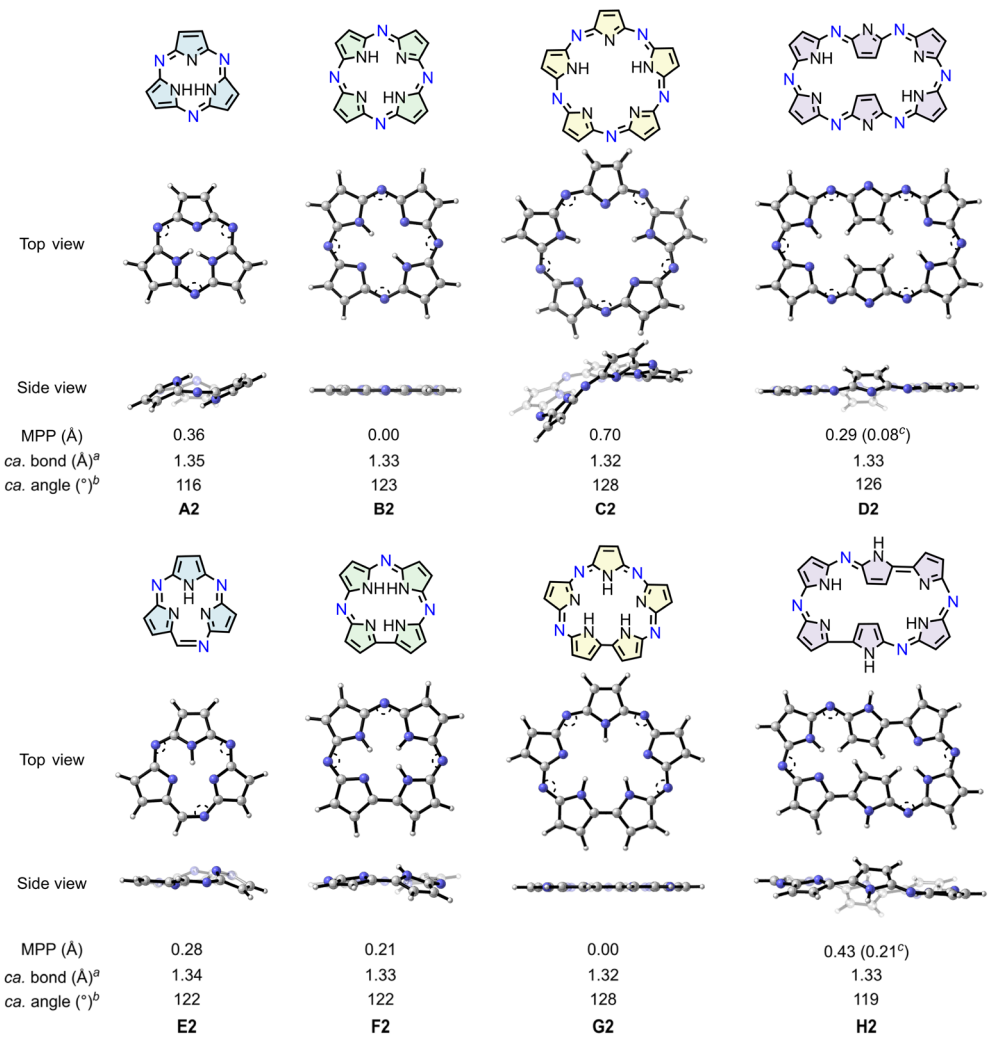

Fig. 3 Optimized geometries of porphyrazine analogues **A2–H2**. [a]Average bond length of all aza-N bridges; [b]average bond angle of all aza-N bridges; [c]C_β atoms of flipped pyrrole rings excluded from MPP calculations.

bridges) remain approximately 1.40 Å, whereas the α-$C_{pyrrole}$–C_{meso}–α-$C_{pyrrole}$ angles vary significantly. The method for calculating the average bond lengths and bond angles of the porphyrin analogues is illustrated in Fig. S1. The average angle increases from 122° in **A1** to 127° in **B1** and 135° in **C1**, indicating a progressive widening of this angle with an increasing number of pyrrole units. However, the average angle in **D1** decreases to 129°, deviating from this trend. This difference may arise from variations in the overall molecular conformation, with **C1** adopting an approximately circular arrangement and **D1** appearing closer to a rectangular geometry. Notably, the geometry of **D1** appears more similar to that of **B1**, which may account for their similar bond angles. An alternative conformation of **D1**, designated **D1-1**, was analyzed to assess the effect of molecular geometry. This structure adopts a circular geometry similar to that of **C1** and shows an average α-$C_{pyrrole}$–C_{meso}–α-$C_{pyrrole}$ angle of 140° (Fig. S2). Computational results indicate that **D1** is 26.3 kcal mol^{-1} lower in energy than **D1-1**, suggesting that **D1** represents the more stable conformation, consistent with experimental observations.[25]

The planarity of these molecules was also evaluated. The molecular planarity parameters (MPP) for **A1–D1** are 0.39, 0.00, 0.00, and 0.22 Å, respectively. The ideal bond angle of a sp^2-hybridized atom is approximately 120°.[26] The average α-$C_{pyrrole}$–C_{meso}–α-$C_{pyrrole}$ angle in **A1** is close to the ideal value, at 122°. However, steric repulsion from the internal NH protons in its small central cavity forces one pyrrole ring to protrude outside the macrocyclic center, reducing the overall planarity. In **B1** and **C1**, the α-$C_{pyrrole}$–C_{meso}–α-$C_{pyrrole}$ angles are slightly larger than 120° and the structures remain relatively stable, possibly due to electronic delocalization. In contrast, two imine-type pyrrole rings in **D1** are flipped, with their nitrogen atoms oriented away from the porphyrin core, introducing additional steric strain and further reducing planarity.

For **E1–H1** (Fig. 2), the average bond lengths and angles of the α-$C_{pyrrole}$–C_{meso}–α-$C_{pyrrole}$ units are comparable to those in **A1–D1**. In addition, the planarity of the structures shows little variation, except for the tri-pyrrole system. Compared with **A1**, **E1** contains an additional carbon atom inserted between two pyrrole units, which enlarges the central cavity of the macrocycle. At the same time, the number of protonated pyrrolic nitrogen decreases to compensate for the additional *meso*-carbons, resulting in a higher degree of planarity for **E1** (MPP = 0.00 Å) compared with **A1** (MPP = 0.39 Å).

The structural effects of different bridging motifs, including *meso*-methine bridges and aza-N bridges, were further examined in porphyrin analogues. The optimized geometries of the porphyrazine analogues **A2–H2**, in which nitrogen atoms occupy the *meso* positions, are shown in Fig. 3. In **A2–H2**, the average α-$C_{pyrrole}$–N_{meso} bond length is approximately 1.33 Å, which is shorter than the corresponding α-$C_{pyrrole}$–C_{meso} bond length in **A1–H1** (about 1.40 Å, Fig. 1 and 2). This difference is consistent with the slightly smaller covalent radius of nitrogen compared to carbon (0.71 Å *vs.* 0.75 Å).[27] Similarly, the average α-$C_{pyrrole}$–N_{meso}–α-$C_{pyrrole}$ angles in **A2–H2** are smaller than the corresponding α-$C_{pyrrole}$–C_{meso}–α-$C_{pyrrole}$ angles in **A1–H1**. These geometric differences affect the overall molecular planarity. Compared to **A1–H1**, the **A2–H2** structures generally show larger MPP values, indicating increased structural distortion.

Among these systems, the structural change is particularly pronounced for **C1** and **C2**: **C1** maintains a planar conformation with a MPP value of 0.00 Å (Fig. 1), whereas **C2** exhibits the largest MPP of 0.70 Å (Fig. 3). This difference is likely associated with increased ring strain arising from a key structural feature: an aza-N bridge linking the two imine-type pyrrole moieties.

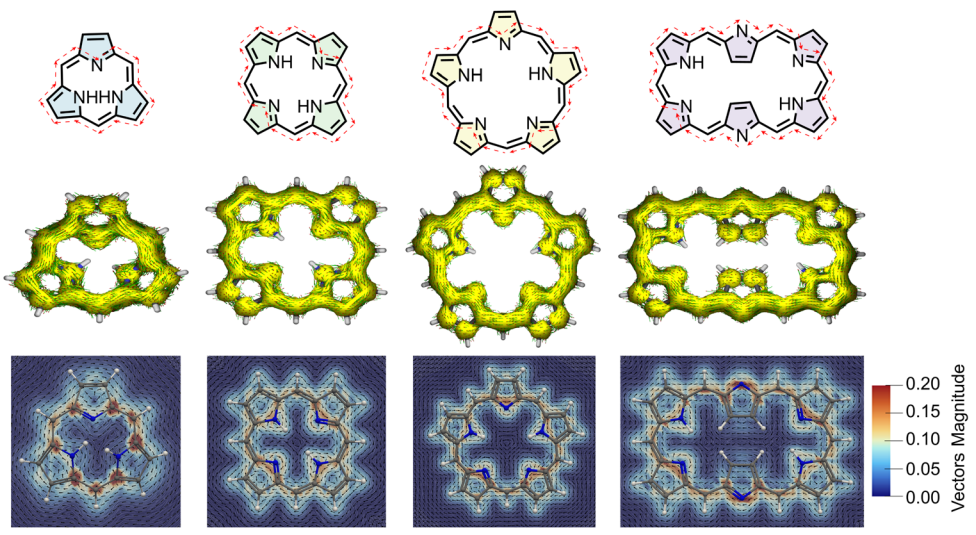

Fig. 4 NICS(1), HOMA values, AICD (isovalue = 0.070), and LIC plots of porphyrin analogues **A1–D1**.

Notably, the bond length of the aza-N bridge is shorter than the corresponding *meso*-methine bridge, leading to steric repulsion between the nitrogen atoms of two imine-type pyrrole rings. To relieve this unfavourable interaction, the fragment undergoes dihedral rotation, causing the two pyrrole rings to deviate from coplanarity and resulting in an overall twisted conformation for **C2**. To examine this hypothesis, geometry optimizations were carried out on two representative fragments. The structure in which an aza-N bridge connects two imine-type pyrrole rings was defined as fragment 1, whereas the structure in which an *meso*-methine bridge connects two imine-type pyrrole rings was defined as fragment 2 (Fig. S3). The optimized structures show that the most stable conformation of fragment 1 adopts a dihedral angle N–C–N–C of −69°, whereas fragment 2 remains nearly planar with a corresponding dihedral angle of −1° (Fig. S3). Fragment 1 adopts a −69° dihedral angle, likely in an effort to relieve unfavourable interaction between the nitrogen atoms of two imine-type pyrrole rings. These results indicate that incorporation of the fragment 1 induces pronounced nonplanar distortion, providing an explanation for the markedly reduced planarity observed for **C2**.

Aromaticity of porphyrin analogues

Studies of aromaticity and antiaromaticity are essential for understanding fundamental molecular properties and reactivity. To evaluate the aromatic character of the porphyrin analogues, NICS values and AICD analyses were calculated. The NICS(1) values at the center of the macrocycle for **A1–H1** are shown in Fig. 4 and 5, and the NICS values for individual pyrrole rings are summarized in Table S1 and Table S2. The calculated NICS(1) values for **A1**, **B1**, **C1**, and **D1** are −13.11, −13.84, −14.86, and −15.08 ppm, respectively. The gradual increase in the magnitude of the NICS(1) values from **A1** to **D1** is primarily attributed to the increasing number of π-electrons. Both NICS scans[28] and harmonic oscillator model of aromaticity (HOMA)[29] values exhibit trends consistent with the NICS(1) results (Fig. 4 and S4). A similar trend is observed for **E1–H1**, with the NICS(1) values following the order **H1** < **G1** < **F1** < **E1**. The dominant current pathways, determined from AICD, line integral convolution (LIC),[30] and bond current strength (BCS)[31] analyses (Fig. S5–S6) and indicated by red lines, are shown in Fig. 4 and 5. AICD and LIC plots show that all porphyrin analogues from **A1** to **H1** exhibit a clockwise ring current. This indicates aromatic character, in good agreement with the NICS results.

A correlation between structural planarity and aromaticity is observed in most systems, with more planar structures generally exhibiting stronger aromatic character (Fig. S7). For example, in the tetra-pyrrole systems, **B1** and **F1** display MPP values of 0.00 and 0.15 Å, respectively, accompanied by NICS(1) values of −13.84 and −12.49 ppm (Fig. 1, 2, 4 and 5).

Although **E1** is more planar than **A1**, with MPP values of 0.00 and 0.39 Å, respectively, its aromaticity is slightly weaker, as indicated by NICS(1) values of −12.21 ppm for **E1** and −13.11 ppm for **A1**. This behavior may be partly explained by the bowl-shaped conformation of **A1**. As reported by Casabianca, molecular curvature can influence aromaticity.[32] In **A1**, the NICS values on the concave and convex sides are −16.34 and −9.88 ppm, respectively (Fig. S8). Compared with the planar structure **E1**, the enhancement of the concave side NICS value in **A1** is more pronounced, ultimately leading to a more negative overall NICS(1) value. In the hexa-pyrrole systems, **D1** and **H1** exhibit significant NICS(1) values of −15.08 and −16.86 ppm, with corresponding MPP values of 0.22 and 0.36 Å, respectively. This result may be related to the placement of the NICS probe (bq), with NICS values calculated at the ring centers defined as

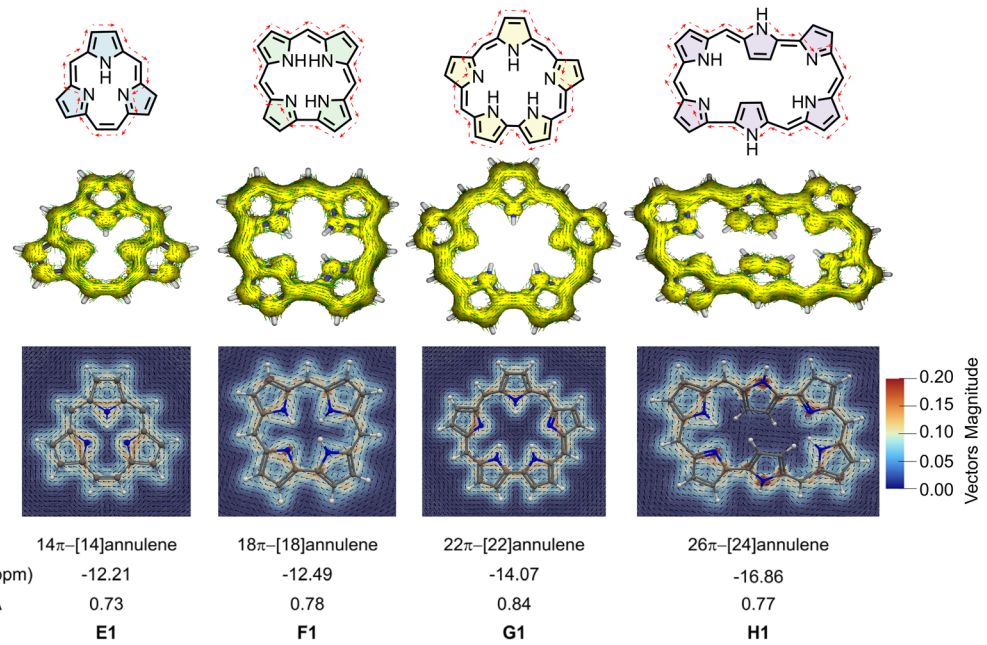

Fig. 5 NICS(1), HOMA values, AICD (isovalue = 0.070), and LIC plots of porphyrin analogues **E1–H1**.

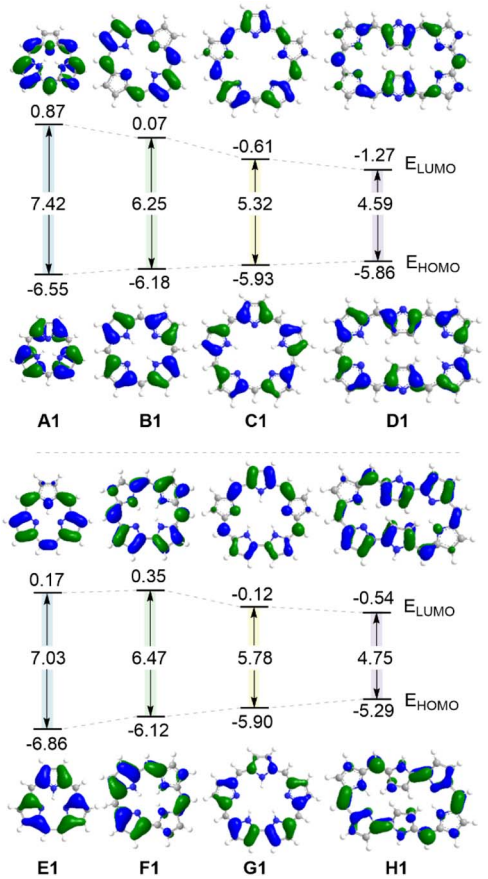

Fig. 6 Molecular orbital distributions and diagrams of the frontier molecular orbitals for A1–H1. The energies are shown in eV.

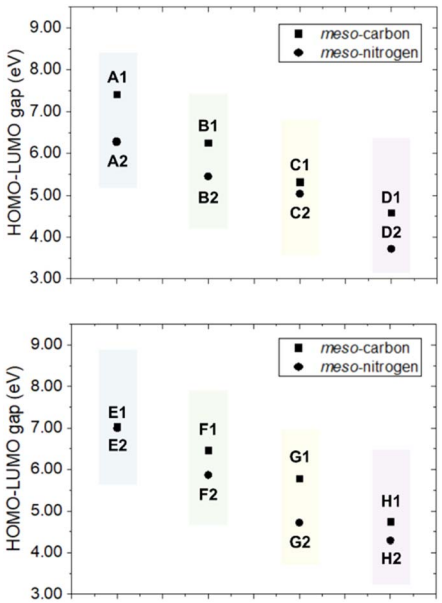

Fig. 7 Plot of HOMO–LUMO energy gap for A1–H1 and A2–H2.

the nonweighted mean of the heavy atom coordinates. In the NICS calculations for **D1** and **H1**, the NICS probe is positioned close to the C_β atoms of the two flipped pyrrole rings. This placement may have a considerable impact on the calculated NICS values. NICS scans show that when the probe is placed more than 1.4 Å from the ring center, the NICS value of **D1** becomes more negative than that of **H1**, indicating relatively stronger aromaticity for **D1**. (Fig. S7).

The porphyrazine analogues with nitrogen at the *meso* positions exhibit NICS(1) values in the range of −17.00 to −10.00 ppm (Table S1), comparable to those of the **A1–H1** series of porphyrin analogues, suggesting that their overall aromatic character remains largely unchanged.

HOMO–LUMO gap of porphyrin analogues

To better understand the influence of structural variations on the electronic properties of these porphyrin analogues, the HOMO–LUMO energy gaps were analyzed, which serve as important indicators of molecular conjugation, optical properties, and electronic stability.[5d] The spatial distributions of the frontier molecular orbitals for porphyrin analogues **A1–D1** are depicted in Fig. 6. For **A1–D1**, the HOMOs are predominantly localized on the pyrrole carbon atoms, corresponding to a_{1u}-type orbitals whereas the LUMOs are mainly distributed over the whole π-conjugated backbone, corresponding to e_g-type orbitals.[33] The calculated HOMO–LUMO energy gaps for **A1–D1** are 7.42, 6.25, 5.32, and 4.59 eV, respectively. As the π-conjugation pathways become longer from **A1** to **D1**, the HOMO–LUMO energy gap decreases. Extension of the π-conjugated system affects both the HOMO and LUMO energy levels, resulting in an increase in the HOMO energy and a decrease in the LUMO energy, with the effect being more pronounced for the LUMO. A clear decrease in the HOMO–LUMO energy gap is also observed from **E1** to **H1**. HOMO–LUMO energy gap calculations performed with other functionals exhibit the same trend (Table S3).

Compared with porphyrin analogues with carbon at the *meso* positions, porphyrazine analogues, in which the *meso*-carbons are replaced by nitrogen, generally exhibit a smaller HOMO–LUMO gap (Fig. 7 and Table S4). In most cases, the narrowing of the HOMO–LUMO gap is primarily associated with stabilization of the LUMO. For instance, the HOMO–LUMO gap decreases from 6.25 eV in **B1** to 5.45 eV in **B2** (Table S4). This reduction is primarily due to a 0.81 eV lowering of the LUMO energy upon substitution of *meso*-carbon atoms by nitrogen, which is likely related to the higher electronegativity of nitrogen (3.04) compared with carbon (2.55).[5b] In contrast, the HOMO energy remains largely unchanged, as the contribution of the *meso* positions to the HOMO orbital is negligible.

Conclusions

In this study, the structural, aromatic, and electronic properties of a series of porphyrin analogues were systematically investigated. Structural analyses reveal that variations in the number of pyrrole units within the macrocyclic framework, as well as differences in bridging motifs, have a pronounced influence on molecular planarity. In particular, incorporation of aza-N

bridges can introduce local steric strain, leading to significant nonplanar distortion in certain analogues. Aromaticity analyses based on NICS and AICD calculations indicate that more planar structures generally exhibit stronger aromatic character, whereas deviations from planarity can noticeably affect aromaticity. Increasing π-conjugation in porphyrin analogues generally raises the HOMO energy and lowers the LUMO energy, resulting in a smaller HOMO–LUMO gap. In addition, substitution of *meso*-carbon atoms by nitrogen typically leads to smaller HOMO–LUMO gaps compared with porphyrin analogues containing *meso*-carbon atoms. We hope that these findings offer guidance for the rational design of functional porphyrin-like systems.

Author contributions

Xiahe Chen: calculation, data curation, and writing – original draft. Dawei Li: calculation, data curation, and writing – original draft. Chengwei Zhang: calculation. Yuanbin She: conceptualization, and project administration. Yun-Fang Yang: conceptualization, supervision, writing – review & editing, and funding acquisition.

Conflicts of interest

There are no conflicts to declare.

Data availability

The data supporting this article have been included as part of the supplementry information (SI). Supplementary information is available. See DOI: https://doi.org/10.1039/d6ra00486e.

Acknowledgements

This work was also supported by the National Natural Science Foundation of China (22371256 and 22138011), the Zhejiang Provincial Natural Science Foundation of China (LR25B020002), the Fundamental Research Funds for the Provincial Universities of Zhejiang (RF-C2022006).

Notes and references

1 (*a*) S. Hiroto, Y. Miyake and H. Shinokubo, *Chem. Rev.*, 2017, **117**, 2910–3043; (*b*) B. Sekaran and R. Misra, *Coord. Chem. Rev.*, 2022, **453**, 214312.

2 (*a*) A. R. Battersby, C. J. R. Fookes, G. W. J. Matcham and E. McDonald, *Nature*, 1980, **285**, 17–21; (*b*) M. Taniguchi and J. S. Lindsey, *Chem. Rev.*, 2017, **117**, 344–535.

3 (*a*) C.-M. Che, V. K.-Y. Lo, C.-Y. Zhou and J.-S. Huang, *Chem. Soc. Rev.*, 2011, **40**, 1950–1975; (*b*) R. Paolesse, S. Nardis, D. Monti, M. Stefanelli and C. Di Natale, *Chem. Rev.*, 2017, **117**, 2517–2583; (*c*) F. Luo, L. Liu, H. Wu, L. Xu, Y. Rao, M. Zhou, A. Osuka and J. Song, *Nat. Commun.*, 2023, **14**, 5028; (*d*) X. Chen, Y.-F. Yang and Y. She, *Org. Chem. Front.*, 2024, **11**, 1039–1049.

4 (*a*) A. Su, C. Zhang, Y.-B. She and Y.-F. Yang, *Catalysts*, 2022, **12**, 1485; (*b*) A. Su, X. Zhang, C. Zhang, D. Ding, Y.-F. Yang, K. Wang and Y.-B. She, *Phys. Chem. Chem. Phys.*, 2023, **25**, 10536–10549; (*c*) S. Fite and Z. Gross, *J. Chem. Inf. Model.*, 2025, **65**, 4403–4411.

5 (*a*) B. Szyszko and L. Latos-Grażyński, *Chem. Soc. Rev.*, 2015, **44**, 3588–3616; (*b*) Y. Matano, *Chem. Rev.*, 2017, **117**, 3138–3191; (*c*) T. Sarma and P. K. Panda, *Chem. Rev.*, 2017, **117**, 2785–2838; (*d*) J. Mack, *Chem. Rev.*, 2017, **117**, 3444–3478.

6 (*a*) C. G. Claessens, D. González-Rodríguez, M. S. Rodríguez-Morgade, A. Medina and T. Torres, *Chem. Rev.*, 2014, **114**, 2192–2277; (*b*) S. Shimizu and N. Kobayashi, *Chem. Commun.*, 2014, **50**, 6949–6966; (*c*) S. Shimizu, *Chem. Rev.*, 2017, **117**, 2730–2784; (*d*) G. Lavarda, J. Labella, M. V. Martínez-Díaz, M. S. Rodríguez-Morgade, A. Osuka and T. Torres, *Chem. Soc. Rev.*, 2022, **51**, 9482–9619.

7 (*a*) B. Szyszko, M. J. Białek, E. Pacholska-Dudziak and L. Latos-Grażyński, *Chem. Rev.*, 2017, **117**, 2839–2909; (*b*) T. Tanaka and A. Osuka, *Chem. Rev.*, 2017, **117**, 2584–2640; (*c*) T. Chatterjee, A. Srinivasan, M. Ravikanth and T. K. Chandrashekar, *Chem. Rev.*, 2017, **117**, 3329–3376; (*d*) Y. Rao, J. Lee, J. Chen, L. Xu, M. Zhou, B. Yin, J. Kim, A. Osuka and J. Song, *Angew. Chem., Int. Ed.*, 2024, **63**, e202409655.

8 (*a*) T. Chatterjee, V. S. Shetti, R. Sharma and M. Ravikanth, *Chem. Rev.*, 2017, **117**, 3254–3328; (*b*) R. Sengupta, M. Ravikanth and T. K. Chandrashekar, *Chem. Soc. Rev.*, 2021, **50**, 13268–13320.

9 (*a*) M. Stępień, N. Sprutta and L. Latos-Grażyński, *Angew. Chem., Int. Ed.*, 2011, **50**, 4288–4340; (*b*) M. Pawlicki and L. Latos-Grażyński, *Chem.–Asian J.*, 2015, **10**, 1438–1451; (*c*) D. W. Thuita and C. Brückner, *Chem. Rev.*, 2022, **122**, 7990–805; (*d*) K. Watanabe, N. N. Pati and Y. Inokuma, *Chem. Sci.*, 2024, **15**, 6994–7009.

10 (*a*) M. Yahya, Y. Nural and Z. Seferoğlu, *Dyes Pigm.*, 2022, **198**, 109960; (*b*) E. Desmedt, D. Smets, T. Woller, M. Alonso and F. De Vleeschouwer, *Phys. Chem. Chem. Phys.*, 2023, **25**, 17128–17142; (*c*) E. Desmedt, M. Jacobs, M. Alonso and F. De Vleeschouwer, *Phys. Chem. Chem. Phys.*, 2025, **27**, 1256–1273.

11 X. Fang, X. Chen, Q. Wang, Y.-F. Yang and Y.-B. She, *Org. Biomol. Chem.*, 2020, **18**, 4415–4422.

12 (*a*) J.-i. Aihara, *J. Phys. Chem. A*, 2008, **112**, 5305–5311; (*b*) H. Fliegl, D. Sundholm, S. Taubert and F. Pichierri, *J. Phys. Chem. A*, 2010, **114**, 7153–7161; (*c*) M. Bröring, *Angew. Chem., Int. Ed.*, 2011, **50**, 2436–2438.

13 (*a*) R. R. Valiev, I. Benkyi, Y. V. Konyshev, H. Fliegl and D. Sundholm, *J. Phys. Chem. A*, 2018, **122**, 4756–4767; (*b*) R. Pino-Rios, G. Cárdenas-Jirón and W. Tiznado, *Phys. Chem. Chem. Phys.*, 2020, **22**, 21267–21274; (*c*) I. Casademont-Reig, T. Woller, V. García, J. Contreras-García, W. Tiznado, M. Torrent-Sucarrat, E. Matito and M. Alonso, *Chem. Eur. J.*, 2023, **29**, e202202264.

14 F. De Vleeschouwer, E. Desmedt and M. Alonso, *Chem. Methods*, 2025, **5**, e202500064.

15 M. J. Frisch, G. W. Trucks, H. B. Schlegel, G. E. Scuseria, M. A. Robb, J. R. Cheeseman, G. Scalmani, V. Barone,

G. A. Petersson, H. Nakatsuji, X. Li, M. Caricato, A. V. Marenich, J. Bloino, B. G. Janesko, R. Gomperts, B. Mennucci, H. P. Hratchian, J. V. Ortiz, A. F. Izmaylov, J. L. Sonnenberg, D. Williams-Young, F. Ding, F. Lipparini, F. Egidi, J. Goings, B. Peng, A. Petrone, T. Henderson, D. Ranasinghe, V. G. Zakrzewski, J. Gao, N. Rega, G. Zheng, W. Liang, M. Hada, M. Ehara, K. Toyota, R. Fukuda, J. Hasegawa, M. Ishida, T. Nakajima, Y. Honda, O. Kitao, H. Nakai, T. Vreven, K. Throssell, J. A. Montgomery Jr, J. E. Peralta, F. Ogliaro, M. J. Bearpark, J. J. Heyd, E. N. Brothers, K. N. Kudin, V. N. Staroverov, T. A. Keith, R. Kobayashi, J. Normand, K. Raghavachari, A. P. Rendell, J. C. Burant, S. S. Iyengar, J. Tomasi, M. Cossi, J. M. Millam, M. Klene, C. Adamo, R. Cammi, J. W. Ochterski, R. L. Martin, K. Morokuma, O. Farkas, J. B. Foresman and D. J. Fox, *Gaussian 16, Revision C.01*, Gaussian, Inc., Wallingford CT, 2019.

16 (*a*) S. Grimme, J. Antony, S. Ehrlich and H. Krieg, *J. Chem. Phys.*, 2010, **132**, 154104; (*b*) S. Grimme, S. Ehrlich and L. Goerigk, *J. Comput. Chem.*, 2011, **32**, 1456–1465; (*c*) J. Witte, N. Mardirossian, J. B. Neaton and M. Head Gordon, *J. Chem. Theory Comput.*, 2017, **13**, 2043–2052.

17 (*a*) D. A. Sharon, D. Mallick, B. Wang and S. Shaik, *J. Am. Chem. Soc.*, 2016, **138**, 9597–9610; (*b*) D. Mallick and S. Shaik, *J. Am. Chem. Soc.*, 2017, **139**, 11451–11459.

18 F. Weigend and R. Ahlrichs, *Phys. Chem. Chem. Phys.*, 2005, **7**, 3297–3305.

19 C. Y. Legault, *CYLview, 1.0b*, Université de Sherbrooke, Canada, 2009, https://www.cylview.org.

20 T. Lu, *J. Mol. Model.*, 2021, **27**, 263.

21 T. Lu and F. Chen, *J. Comput. Chem.*, 2012, **33**, 580–592.

22 F. Weigend, *Phys. Chem. Chem. Phys.*, 2006, **8**, 1057–1065.

23 (*a*) P. v. R. Schleyer, C. Maerker, A. Dransfeld, H. Jiao and N. J. R. van Eikema Hommes, *J. Am. Chem. Soc.*, 1996, **118**, 6317–6318; (*b*) Z. Chen, C. S. Wannere, C. Corminboeuf, R. Puchta and P. v. R. Schleyer, *Chem. Rev.*, 2005, **105**, 3842–3888; (*c*) T. Stuyver, M. Perrin, P. Geerlings, F. De Proft and M. Alonso, *J. Am. Chem. Soc.*, 2018, **140**, 1313–1326.

24 (*a*) R. Herges and D. Geuenich, *J. Phys. Chem. A*, 2001, **105**, 3214–3220; (*b*) D. Geuenich, K. Hess, F. Köhler and R. Herges, *Chem. Rev.*, 2005, **105**, 3758–3772.

25 (*a*) L. Simkhovich, I. Goldberg and Z. Gross, *Org. Lett.*, 2003, **5**, 1241–1244; (*b*) M. Suzuki and A. Osuka, *Org. Lett.*, 2003, **5**, 3943–3946.

26 M. Diociaiuti, S. Casciardi and R. Sisto, *Micron*, 2016, **90**, 97–107.

27 P. Pyykkö and M. Atsumi, *Chem. Eur. J.*, 2009, **15**, 186–197.

28 (*a*) A. Stanger, *J. Org. Chem.*, 2006, **71**, 883–893; (*b*) A. Espinosa Ferao, *Inorg. Chem.*, 2025, **64**, 11832–11844.

29 (*a*) J. Kruszewski and T. M. Krygowski, *Tetrahedron Lett.*, 1972, **13**, 3839–3842; (*b*) T. M. Krygowski, *J. Chem. Inf. Comput. Sci.*, 1993, **33**, 70–78.

30 (*a*) J. Jusélius, D. Sundholm and J. Gauss, *J. Chem. Phys.*, 2004, **121**, 3952–3963; (*b*) H. Fliegl, S. Taubert, O. Lehtonen and D. Sundholm, *Phys. Chem. Chem. Phys.*, 2011, **13**, 20500–20518.

31 G. Monaco, F. F. Summa and R. Zanasi, *J. Chem. Inf. Model.*, 2021, **61**, 270–283.

32 L. B. Casabianca, *J. Phys. Chem. A*, 2016, **120**, 7011–7019.

33 (*a*) S. I. Yang, J. Seth, T. Balasubramanian, D. Kim, J. S. Lindsey, D. Holten and D. F. Bocian, *J. Am. Chem. Soc.*, 1999, **121**, 4008–4018; (*b*) R.-J. Cheng, P.-Y. Chen, T. Lovell, T. Liu, L. Noodleman and D. A. Case, *J. Am. Chem. Soc.*, 2003, **125**, 6774–6783.